METALS AND MATERIALS, Vol. 2, No. 1 (1996), pp. 49~64

Grain Boundary Segregation and Intergranular Fracture in Ferrite Containing Mo, Si or Al

N. H. HEO

Department of Materials Science and Engineering, Massachusetts Institute of Technology, Cambridge, MA 02139, U.S.A.

Roles of molybdenum, silicon or aluminum in ferrite on grain boundary segregation and hence on intergranular fracture have been investigated by using Auger electron spectroscopy (AES) and tensile test. Competitive segregation between sulfur and carbon or nitrogen, which caused the decrease below 700°C of sulfur content at the grain boundaries, was observed in the pure iron. The intergranular brittleness of the pure iron was caused by sulfur at the grain boundaries. When molybdenum was added to the pure iron, the sulfur contents at the grain boundaries were lowered in comparison to those in the pure iron. The molybdenum-bearing alloy showed higher fracture strength than that of the pure iron, and fractured mostly in the transgranular mode. This arises from the intrinsic effect of molybdenum on the grain boundaries as well as the decrease in sulfur content. In the 3.37 wt.%Si alloy, silicon and carbon or nitrogen competitively segregated to the grain boundaries, and such a competitive segregation was also observed between sulfur and carbon or nitrogen. The sulfur content at the grain boundaries decreased with increasing silicon content. The fracture modes in the 3.37- and 4.26 wt.%Si alloys were transgranular in the rolling direction, but were mostly intergranular in the transverse direction and in the as-rolled condition. The intergranular characteristic in the fracture behavior may be attributed to the detrimental effect of silicon as well as sulfur on the intergranular cohesion. Carbon and aluminum only were found at the grain boundaries of the aluminum-bearing alloy. This suggests that aluminum is a strong repulser of sulfur or nitrogen at the grain boundaries. Additionally, it was found that aluminum has a detrimental effect on grain boundary strength of ferrite.

1. INTRODUCTION

Because grain boundary segregation influences many mechanical and chemical properties of materials [1], great attention has been paid to the study of grain boundary segregation in connection to the properties mentioned.

Molybdenum has been shown to inhibit temper embrittlement, not only in steels containing phosphorus, but also in steels containing the other known embrittling elements, including manganese [2]. A study of Fe-Mo-P alloys [3] led to the conclusion that the benificial effect of molybdenum resulted from an enhancement of carbon segregation. A direct scavenging of phosphorus in solid solution by molybdenum remains a possibility, as does the suggestion of Dumoulin *et al.* [4] that molybdenum decreases the embrittling potency of phosphorus. This effect would only operate as long as there is enough molybdenum in solid solution to cosegregate to grain boundaries with carbon. Several long-time aging studies [2, 5, 6] showed that the beneficial effect of molybdenum ultimately disappeared when the molybdenum was precipitated in alloy carbides. Furthormore, a study of NiCrMo steels showed that molybdenum appeared to decrease tin segregation as well as phosphorus segregation [7].

The study of Fe-Si alloys is of general interest because Si is a common alloying element for steels and influences several material properties. Fe-Si alloys with 3-4 wt.% Si are widely used as industrial transformer steels, where grain orientation improves the magnetic properties. Addition of Si may improve the resistance to stress corrosion cracking [8], and is assumed to have as well a benificial as a detrimental effect on secondary hardening of steels [9]. In all these cases, interfacial segregation phenomena are suspected to play a significant role. Repulsion or cosegregation at surfaces or grain boundaries between Si and impurities has been reported in Fe-Si alloys [10-18]. Aluminum decreases the activity of carbon in ferrite and increases it in cementite, both effects acting to retard cementite precipitation [19]. Addition of small amounts of Si alters the hardening

response, the toughness and the fracture characteristics of secondary hardening steels by affecting both the precipitate sites and morphology and by segregation of the Si itself to prior austenite grain boundaries at temperatures beyond the peak hardening temperature [9]. The deleterious effect of Si, i.e. its enhancement of temper embrittlement, can be significantly lessened by substitution, in part, by the element Al.

In this paper, mechanical properities of pure iron after aging are first examined related to the grain boundary segregation of impurities. Effects of addition to the pure iron of an alloying element such as Mo, Si or Al on the grain boundary segregation behavior of impurities and hence on the mechanical properties are investigated.

2. THEORETICAL BACKGROUNDS OF GRAIN BOUNDARY SEGREGATION

2.1. Driving force for interfacial segregation

Over the past two decades, the results of surface segregation measurements have almost invariably been interpreted by means of models in which a decrease in surface free energy is assumed to be the predominant driving force for the segregation process [20]. In concrast, the interpretation of grain boundary segregation experiments has generally been based on the assumption that a decrease in lattice strain energy, associated with misfitting solute atoms, provides the driving force for the process [21]. It is clear, however, that any complete of equilibrium interfacial composition must involve minimization of the total system free energy, which includes contributions from both interfacial free energy and the lattice solute energy strain of the alloy.

When considered separately, the surface free energy and solute strain energy effects can lead to qualitatively different predictions of the component which segregates to the surface of a dilute binary alloy. For example, in a hypothetical, ideal A-B solid solution in which the pure component A possesses a lower surface energy than pure component B, minimization of surface free energy would dictate a higher concentration of A in the surface than in the bulk of the alloy, for all bulk compositions of the alloy. In constrast, the solute strain energy concept would predict a higher concentration of the solute in the surface than in the bulk. Thus, the two effects would tend to reinforce one another in the case of a B-rich alloy whereas they would tend to counteract one another in an A-rich alloy.

Most of the microscopic statistical treatments of interfacial segregation [22-28] in solid solutions assume a "two-phase" model, consisting of a bulk phase and an interface phase. In a crystal consisting of a two-component solid solution in which the first atom plane is taken to be the surface phase, the atom fractions [21, 22, 26, 29] of components A and B in the surface phase, X_A^s and X_B^s, can be expressed as follows:

$$\frac{X_A^s}{X_B^s} = \frac{X_A^b}{X_B^b}\exp\left(\frac{-\Delta G_a}{kT}\right) = \frac{X_A^b}{X_B^b}\exp\left(\frac{\Delta S_a}{k}\right)\exp\left(\frac{-\Delta H_a}{kT}\right) \tag{1}$$

where X_A^b and X_B^b are the corresponding quantities for the bulk phase, ΔF_a and ΔS_a are the free energy and entropy of adsorption respectively, ΔH_a is the enthalpy or heat of adsorption of the segregating component. The enthalpy of adsorption [22, 30] is given by

$$\Delta H_a = (\gamma_A - \gamma_B)A + \frac{2\Delta H_m}{ZX_A^bX_B^b}\left\{Z_l(X_A^b - X_A^s) + Z_v(X_A^b - \frac{1}{2})\right\} - \left\{\frac{24\pi kGr_0r_1(r_0 - r_1)^2}{3Kr_1 + 4Gr_0}\right\} \tag{2}$$

where γ_A and γ_B are the surface energies of components A and B respectively, A is the surface area per atom, Z_l is the number of lateral bonds made by an atom within its plane, Z_v is the number of bonds made by an atom to each adjacent plane of atoms (e.g. for an fcc crystal with a {111}-type surface, Z_l=6 and Z_v=3), K is the bulk modulus of the solute, G is the shear modulus of the solvent, r_0 is the radius of the solvent atom in the pure solvent and r_1 is the radius of the solute atom in the pure solute. In equation (11), the right first and second terms are related to surface energy [22], and the third term arises from lattice strain energy [30] associated with misfitting solute atoms and is the easier expression for evaluation of strain energy than that employed by McLean [21].

To the same degree of approximation as equation (2), the entropy of adsorption can be written by

$$\Delta S_a = (S_A - S_B)A + \frac{2\Delta S_m^E}{ZX_A^bX_B^b}\left\{Z_l(X_A^b - X_A^s) + Z_v(X_A^b - \frac{1}{2})\right\} + \frac{\partial}{\partial T}\left\{\frac{24\pi kGr_0r_1(r_0 - r_1)^2}{3Kr_1 + 4Gr_0}\right\} \tag{3}$$

where S_A and S_B are the specific surface entropies of the pure components.

2.2. Theory of grain boundary segregation

The theories of equilibrium segregation are derived from the grain boundary analogue of Langmuir adsorption at free surfaces [21,31] as follows

$$\frac{X_I}{X_I^0 - X_I} = \frac{X_I^B}{1 - X_I^B} \exp\left(-\frac{\Delta G_I}{RT}\right) \tag{4}$$

The standard Langmuir-McLean equation (4) is valid for the binary solid solution M-I. The term X_I^0 represents the fraction of the grain boundary monolayer available for segregated atoms at saturation, and is usually replaced by 1, X_I is the fraction of grain boundary covered with the atoms of segregant, X_I^B is the fraction of segregant atoms in the bulk, and ΔG_I is the free energy of segregation per mole of solute and can be written as

$$\Delta G_I = \Delta H_1 - T\Delta S_I \tag{5}$$

where ΔH_I is the segregation enthalpy and ΔS_I is the segregation entropy.

Gupta and Perraillon [32] expressed the equilibrium grain boundary concentration of I and M in ternary Fe-M-I system through

$$\frac{X_i}{1 - X_I - X_M} = \frac{X_i^B}{1 - X_I^B - X_M} \exp\left(-\frac{\Delta G_i}{RT}\right), \quad i = I, M \tag{6}$$

Equation (6) is equivalent to the Guttmann's equation [33] derived before Gupta and Perraillon. The terms ΔG_i, i=I, M represent the free energies of segregation in ternary system and take the forms:

$$\begin{aligned} \Delta G_I &= -\Delta G_I^0 + 2\alpha_{FeI}(X_I - X_I^B) - \alpha'_{MI}(X_M - X_M^B) \\ \Delta G_M &= -\Delta G_M^0 + 2\alpha_{FeM}(X_M - X_M^B) - \alpha'_{MI}(X_I - X_I^B) \end{aligned} \tag{7}$$

where ΔG_I^0 and ΔG_I^0 are free energies of segregation for I and M in their respective binary systems with Fe, α^*_{MI} is the relative chemical interaction energy between solute atoms M and I with respect to the solvent Fe according to

$$\alpha'_{MI} = \alpha_{MI} - \alpha_{FeI} - \alpha_{FeM}. \tag{8}$$

Since α'_{MI} is usually greater than α_{FeI} or α_{FeM} [34], the binary Fowler's terms (α_{FeI}, α_{FeM}) in equation (7) are frequently ignored for simplicity, and then the second term in the right hand side of equation (7) disappears. Equation (6) is valid only for competitive equilibrium segregation (I and M atoms segregate on the same sets of sites). A positive value of α' expresses a relative attraction between I and M dissolved in Fe, whereas α'<0 means a relative repulsion between I and M (or a relative attraction between I-I and M-M). Assuming a non-competitive segregation [34, 35], equation (6) reduces to the following equation, which is equivalent to equation (4):

$$\frac{X_i}{1 - X_i} = \frac{X_i^B}{1 - X_i^B} \exp\left(-\frac{\Delta G_i}{RT}\right), \quad i = I, M \tag{9}$$

where has the same meaning as in the previous case.

Yu and McMahon [36] modified equation (7) for a multicomponent system. They expressed the free energy of segregation in such system as

$$\Delta G = -\Delta G_i^0 + 2\alpha_{Fei}(X_i - X_i^B) - \sum_{j \neq i} \alpha'_{ji}(X_j - X_j^B). \tag{10}$$

2.3. Kinetics of grain boundary segregation

2.3.1. Grain boundary segregation with no precipitation reaction

In practical situations where segreation is important, the segregant atoms often have insufficient time to reach their full equilibrium level as defined by the adsorption theories. Most models of the kinetics follow McLean's approach [21]. Solute atoms are assumed to segregate to a grain boundary from two infinite half-crystals of uniform solute content or to a surface from one infinite half-crystal. Diffusion in the crystals is described by Fick's laws and the ratio of the concentration of the solute in the grain boundary to that in the adjacent atom layer of the bulk is given by the constant enrichment ratio β. The kinetics of the segregation are thus described by

$$\frac{X_b(t) - X_b(0)}{X_b(\infty) - X_b(0)} = 1 - \exp\left(\frac{FDt}{\beta^2 f^2}\right) \cdot erfc\left(\frac{FDT}{\beta^2 f^2}\right)^{1/2} \tag{11}$$

where F=4 for grain boundaries and 1 for the free surface, $X_b(t)$ is the boundary content at time t, b is the solute bulk diffusivity and f is related to the atom sizes of the solute and matrix, b and a respectively, by f=a^3b^{-2}. For short times equation (11) approximates to

$$\frac{X_b(t) - X_b(0)}{X_b(\infty) - X_b(0)} = \frac{2b^2}{\beta a^3}\sqrt{\frac{FDt}{\pi}}. \tag{12}$$

Equations (11) and (12) are, in fact, limited extremes of a general problem. In practice, β is constant only for dilute systems with low segregation levels. As segregation increases β generally falls as a result of saturation. If β starts high and falls rapidly as the segregation saturates, equation (12) is valid up to saturation [37, 38]. A de-

tailed analysis for the saturation occurring in the Langmuir-McLean adsorption theory has been presented by Rowlands and Woodruff [39]. Their analysis shows how the time dependence of the segregation changes from equation (11) to equation (12) as the final equilibrium segregation level $X_b(\infty)$ approaches the saturation level $X_b(0)$.

The above discussions are valid for wholly enclosed surfaces or for grain boundaries. For surface segregation experiments in a vacuum system using AES, evaporation of the segregant may occur. Lea and Seah [37, 40] evaluated the effect of surface evaporation concomitant with surface segregation with the following equation:

$$\frac{X_s(t)-X_s(0)}{X_s(\infty)-X_s(0)}=\frac{1}{E+1}\exp\left(\frac{Edt}{\beta^2 f^2}\right)\left[1-\exp\left(\frac{(E+1)Dt}{\beta^2 f^2}\right)\cdot erfc\left(\frac{Dt}{\beta^2 f^2}\right)^{1/2}-(E)^{1/2}erf\left(-\frac{EDt}{\beta^2 f^2}\right)^{1/2}\right] \quad (13)$$

where E is the dimensionless parameter related to evaporation rate. The results show no divergence initially from the McLean result of equation (11). However, as the segregation builds up, the evaporation rate increases and the bulk material begins to be depleted of solute. The segregation goes through a maximum and eventually irreversibly falls to a low value as the substrate purifies.

2.3.2. Grain boundary segregation with precipitation reaction

If the segregating element does not form a precipitate with an element within the matrix, its segregation based on equations (4) or (6) increases with increasing bulk concentration and decreasing temperature, following equations (11) or (12). An example of this effect is seen for phosphorus segregation in iron [41].

If a precipitate is formed, the amount of segregation will not increase with increasing bulk concentration once the solubility limit has been exceeded at any given temperature.

Recently, Heo and Lee [42] observed the grain boundary segregation and subsequent desegregation phenomena of elements in Fe-Mn-Ni ternary alloys durng isothermal aging, which are directly governed by the MnNi precipitation reaction in the matrix. More recently, Heo analyzed theoretically the phenomena in the basis of a regular solution model [43, 44]. According to the Heo's results, the segregation kinetics of the elements in ternary alloys, which are accompanied by a precipitation reaction of the elements, can be described by the following equation:

$$X_b(t)=X_b(\infty)-\{X_b(\infty)-X_b(0)\}\exp\left(\frac{4Dt}{\beta^2 f^2}\right)erfc\left(\frac{4Dt}{\beta^2 f^2}\right)^{1/2}-\beta P(t)+\beta\int_0^t P'(t-u)\exp\left(\frac{4Dt}{\beta^2 f^2}\right)erfc\left(\frac{4Dt}{\beta^2 f^2}\right)^{1/2}du \quad (14)$$

where $P(t)$ is a function related to the precipitaiton reaction within the matrix, $P'(t)$ is the time derivative of $P(t)$. Without any precipitation in the matrix (i.e., if $P(t=0)$, equation (14) reduces to the McLean's equation [21] expressed by equation (11). Otherwise, the right third and fourth terms in equation (14) have a negative effect on the segregation kinetics to the grain boundaries, and hence have a similar effect to evaporation.

2.4. Quantification methods of surface composition

Several methods of determination of the surface composition are based on the model of single layer segregation [47-51]. It is generally assumed in these methods that the segregation is concentrated in the top atomic layer whereas the composition of the other layers is homogeneous and equals the bulk composition. The expressions based on equation (5) in Table 1 describe a surface enrichment only in a dilute binary alloy, while both enrichment and depletion may be determined by means of the more general expressions (3) and (4) in Table 1. The model of single layer segregation is a very useful tool for the description of the adsorption behaviour. However, if the composition varies in more layers, even this model can not be used rigorously.

The methods of calculations of surface composition respecting a heterogeneous distribution of elements in several surface layers, seem to give results which reflect reality in the best way. The "multilayer segregation" approach includes information about the composition below the surface. This information can be represented either by the Auger peak heights (APH) of individual elements measured after removal of the top atomic layer [52, 53] (equation (5a) and (5b) in Table 1) or by the derivative of the APH depth profiles at the surface [54] (equation (6) in Table 1). Evidently, the methods of "multilayer segregation" can be also applied to both to the case of homogeneous distribution of elements in the vicinity of the surface (e.g. $I_j^M(0)=I_j^M(d^M)$) and to the case of single layer segregation ($I_j^M(d^M)=0$) or depletion ($I_j^M(d^M)=I_j^b$).

3. EXPERIMENTAL PROCEDURES

Table 1. Calculation methods of surface composition

Model of calculation	Expression		Ref.
Homogeneous distribution	$X_A^M = \{F_A I_A^M(0)\}/\{\sum_j F_j I_j^M(0)\}$	(1)	
	$F_j = 1/I_j^s$	(1a)	[45]
	$F_j = \{n_j^s[1+r^s(E_j,\alpha)]\lambda^s(E_j,\theta)\}/\{I_j^s[1+r^M(E_j,\alpha)]\lambda^M(E_j,\theta)\}$	(1b)	[46]
Single layer segregation	$X_A^M = \{Q_{BA}^A I_A^M(0)/I_A^s\}\{I_B^M(0)/I_B^s\}$	(2)[a]	
	$Q_{BA}^A = \lambda^M(E_A,\theta)$	(2a)	[47]
	$Q_{BA}^A = \{[1+r^s(E_A,\alpha)]/a_A^{1.5}\}/\{[1+r^M(E_A,\alpha)]/a_B^{1.5}\}$	(2b)	[48]
	$Q_{BA}^A = \{1-\exp[-d^M/\lambda^M(E_A,\theta)]\}/\{1-\exp[-d^M/\lambda^M(E_B,\theta)]\}$	(2c)	[49]
	$X_A^M = \frac{1}{1-\exp[-d^M/\lambda^M(E_A,\theta)]}\cdot\frac{I_A^M(0)/I_A^s}{\sum_j I_j^M(0)/I_j^s} - \frac{I_A^b(0)/I_A^s}{\sum_j I_j^b(0)/I_j^s}\exp[-d^M/\lambda^M(E_A,\theta)]$	(3)	[50]
	$\frac{X_A^M + \sum_{k=0}^{\infty} X_A^b \exp[-kd^M/\lambda^M(E_A,\theta)]}{(1-X_A^M)+\sum_{k=0}^{\infty}(1-X_A^b)\exp[-kd^M/\lambda^M(E_B,\theta)]} = \frac{I_A^M(0)I_B^s n_B^s[1+r^s(E_A,\alpha)]\cdot[1+r^M(E_B,\alpha)]}{I_B^M(0)I_B^s n_B^s[1+r^s(E_B,\alpha)]\cdot[1+r^M(E_A,\alpha)]}$	(4)[b]	[51]
Multilayer segregation	$X_A^M = \left[F_A\{I_A^M(0)-I_A^M(d^M)\exp[-d^M/\lambda^M(E_A,\theta)]\}\right]/\{1-\exp[-d^M/\lambda^M(E_A,\theta)]\} \times\left[\sum_j F_j\{I_j^M(0)-I_j^M(d^M)\exp[-d^M/\lambda^M(E_j,\theta)]\}/\{1-\exp[-d^M/\lambda^M(E_j,\theta)]\}\right]^{-1}$	(5)	
	$F_j = n_j^s/I_j^s,\ F_j = 1/I_j^s$	(5a, 5b)	[52, 53]
	$X_A^M = F_A\left\{I_A^M(0)-\lambda^M(E_A,\theta)\left(\frac{\partial I_A^M}{\partial z}\right)_{z=0}\right\}/\sum_j F_j\left\{I_j^M(0)-\lambda^M(E_j,\theta)\left(\frac{\partial I_{ij}^M}{\partial z}\right)_{z=0}\right\}$	(6)[c]	[54]
	$F_j = \{n_j^s[1+r^s(E_j,\alpha)]\lambda^s(E_j,\theta)\}/\{I_j^s[1+r^s(E_j,\alpha)]\lambda^M(E_j,\theta)\}$		

[a] Dilute binary alloy A-B.

[b] Binary alloy A-B.

[c] Originally derived for ESCA technique. In the case of AES the back-scattering factors have been included in this formula.

Simbols used: X_A^M surface concentration of element A (in at.%), I_j^M (0); APH of element j measured at the surface, $I_j^M(d^M)$; APH of element j measured at the new surface after removal of one atomic layer of thickness d^M, I_j^b: APH of element j measured in the bulk, I_j^s: relative sensitivity factor of element *j*, n_j: atomic density of element *j*, $r(E_j, \alpha)$: back-scattering factor corresponding to kinetic energy E_j of an Auger electron of element *j* and to angle α of the incident primary electron beam to the target, $\lambda(E_j, \theta)$: the escape depth of Auger electrons of element *j*, θ: (mean) angle of detected Auger electrons to the target, a_j: lattice parameter of element *j*, *E*: probability of penetration of an Auger electron into the layer immediately above, *k*: the depth variable. Superscripts M, s and b correspond to the alloy, to the pure standard and to the bulk, respectively.

3.1. Preparation of alloys

Pure iron, 1.9Mo-, 3.37Si- 4.26Si- and 4.7Al-bearing alloys were prepared from vacuum induction melting using electrolytic iron, pure aluminum balls and molybdenum brickets. The alloys were homogenized and hot-rolled to 2.5 mm plates. After decarburization treatment at 730°C for 18 h under wet hydrogen atmosphere and subsequently at 900°C for 3 h in the same atmosphere, followed by water quenching, the alloys were baked at 200°C for 4 h in order to minimize the hydrogen effect on the grain boundaries. The alloy containing 4.26 wt.% Si were, however, heat-treated at the same temperatures with argon atmosphere. The five alloys each contained 0.0022, 0.0019, 0.0038, 0.0037 and 0.0028 wt.% S, and contained 0.0014, 0.0029, 0.0036, 0.0017 and 0.0009 wt.% C. The alloys were aged for various times (i.e. 160 h at 450, 500 and 550°C, 20 h at 600°C, 1h at 700, 800 and 900°C) in a neutral salt bath. Hardness tests were performed on the aged alloys, and tensile tests were also carried out in liquid nitrogen on samples machined in the rolling direction and having a dimension (25 mm in gauge, 6.25 mm in width and 1.8 mm in thickness).

3.2. Auger electron spectroscopy

In order to investigate grain boundary segregation behaviors of solutes, AES samples, machined from tensile specimens and chilled with liquid nitrogen, were fractured in an ultra high vacuum chamber of about 1×10^{-7} Pa. An incident beam energy of 5 KeV was used, and the beam diameter was approximately 1 mm. About 10 grain boundary facets from each sample were used to obtain one datum point. The sulfur 150 eV, nitrogen 379 eV, carbon 272 eV and phosphorus 120 eV peaks were selected for the analyses. Molybdenum, silicon and aluminum peaks each were 186, 92 and 1396 eV. All the differential Auger peaks were normalized by the iron 703 eV peak. It should be noted that the silicon 92 eV peak contains a contribution of uncertain magnitude from the iron 86 eV peak and that the latter decreases rapidly as the iron is covered by segregating elements. Normalized peaks were converted to monolayer fractions according to the Heo's equation [43] of which the derivation is shown in the Appendix of the present study:

$$I_X = I_{X,0}[(f_X - f_{X,0})\{1 - \exp(-1/\lambda_X \cos\theta)\} + f_{X,0}]$$

$$I_{Fe} = I_{Fe,0}\left\{1 - \sum_{X \neq Fe}^{N} f_X + \sum_{X \neq Fe}^{N} (f_X - f_{X,0}) \exp(-1/\lambda_{Fe} \cos\theta)\right\} \quad (15)$$

and

$$\frac{I_{X,0}}{I_{Fe,0}} = \frac{S_X}{S_{Fe}} \quad (16)$$

where f_X is the monolayer mole fraction of an element X in iron-base alloy system; λ_X and λ_{Fe} indicate the inelastic mean free paths (IMFP) in monolayers of the X and Fe Auger electrons; υ is the emission angle of the Auger electrons to the surface normal; S_X and S_{Fe} are the relative sensitivity factors between the pure elements and silver, obtained from the Handbook of Auger Electron Spectroscopy [45]; I_X and I_{Fe} are the Auger peak amplitudes of the element X and the bulk Fe, respectively; $I_{X,0}$ and $I_{Fe,0}$ are the intensities of the relative signals from the pure bulk samples; $f_{X,0}$) is the mole fraction of X in the bulk. The value of cosυ in equation. (15) can be replaced by 0.74 [55, 56]. In the previous research [42], a similar equation to equation (15), which does not contain cosυ in the numerator of the exponential term, was used for quantifying AES peaks, but equation (15) is suggested for better results. The IMFP of the X Auger electron was evaluated by using the equation of Seah and Dench [57]:

$$\lambda_X = \frac{538}{E_X^2} + 0.41(aE_X)^{1/2} \text{ (in monolayers)} \quad (17)$$

where E_X (between 1 and 10,000 eV above the Fermi level) is the Auger electron energy in eV for the element X, a is the monolayer thickness in nanometres of the X element given by

$$a^3 = \frac{A}{\rho n N} \quad (18)$$

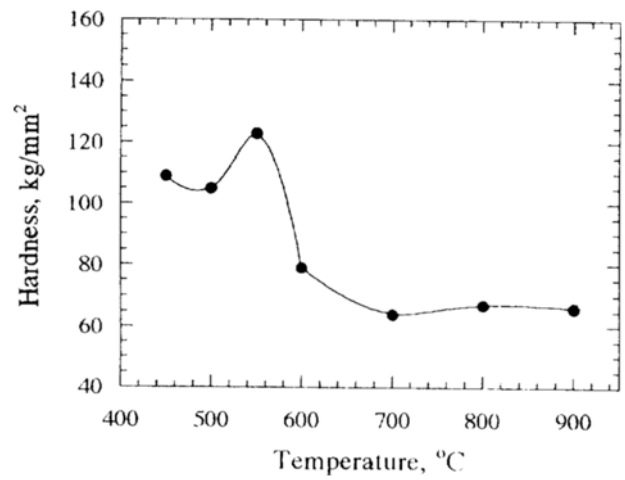

Fig. 1. Changes in hardness of the decarburized pure iron with aging temperature.

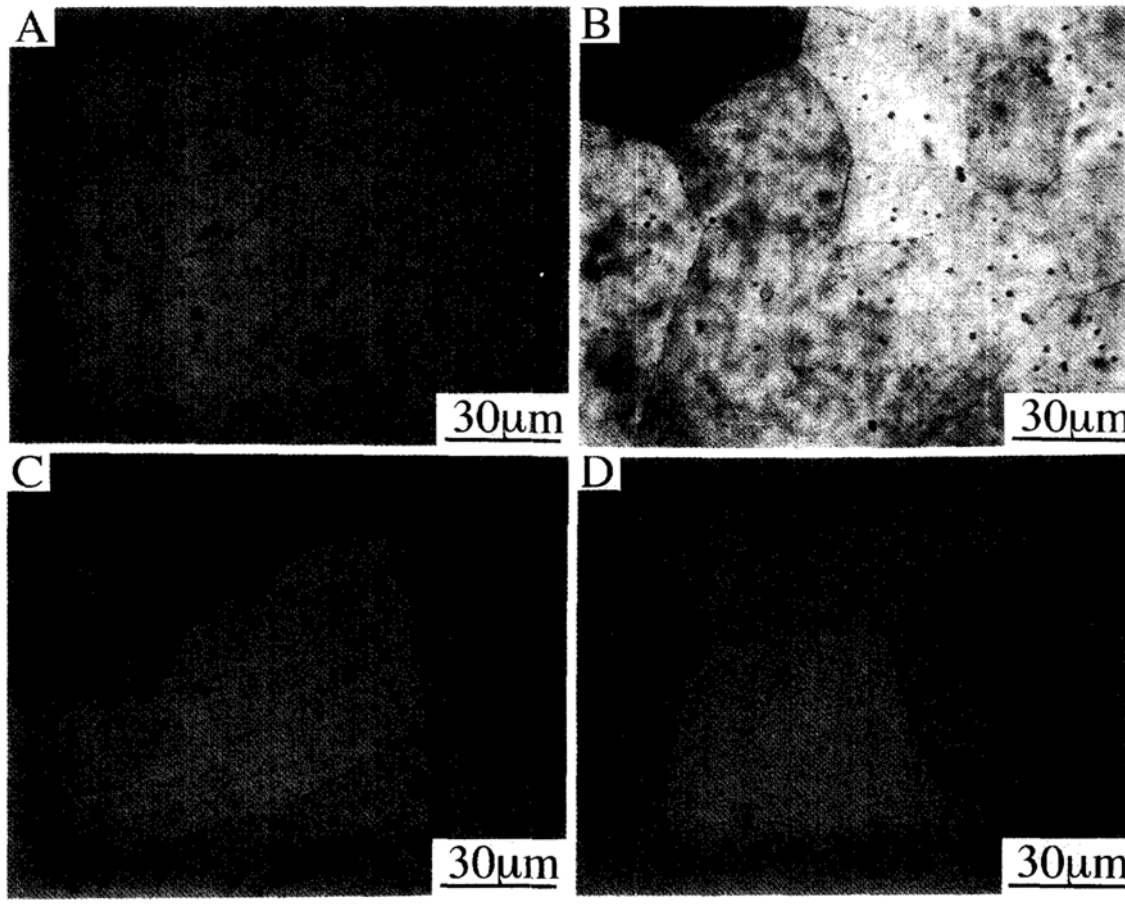

Fig. 2. Microstructures of four alloys after aging: (a) the pure iron aged at 550°C, (b) the molybdenum-bearing alloy aged at 500°C, (c) the 3.37 wt.% Si alloy aged at 550°C and (d) the aluminum-bearing alloy aged at 550°C.

where A is the atomic or molecular weight, n is the number of atoms in the molecule, N is Avogadro's number and ρ is the bulk density [58, 59].

4. RESULTS

Changes in hardness of decarburized pure iron with aging temperature is shown in Figure 1. The pure iron showed various hardness levels with aging temperature: about Hv 115 below 550°C, a maximum hardness of Hv 123 at 550°C and approximately Hv 70 above 600°C. It was reported in a previous research [60] that an undecarburized pure iron was age-hardened by oxide, and showed a maximum hardness of Hv 230 at 550°C. As a result, the maximum hardness in the present decarburized pure iron is considerably low in comparison to that in the undecarburized pure iron. This may be attributed to a decrease in oxygen content necessary to the age-hardening after decarburization treatment, though a research [61] reported little change in oxygen content of pure iron after decarburization treatment. Figure 2 shows microstructures of four alloys containing the decarburized pure iron. Oxide particles not uniform in size can be seen at the grain boundaries and in the matrix of the pure iron. The molybdenum-bearing alloy also contained many oxide particles after aging, but oxide particles were little found in the silicon- and aluminum-bearing alloys. This is because the silicon or the aluminum contained acted as a strong deoxidizer during melting process.

The ultimate tensile strength and elongation of the pure iron vary also with aging temperature, as shown in Figure 3. Some elongation was obtained after aging at 800 and 900°C, but the pure iron, irrespective of its lower hardness, exhibited a severe embrittlement at 600 and 700°C, in which the tensile strengths were about 270 MPa. From 700°C, the ultimate tensile strength drastically increased with decreasing temperature, and, at 500°C, amounted to 630 MPa, a maximum tensile strength. At 450°C, the pure iron showed a relatively de-

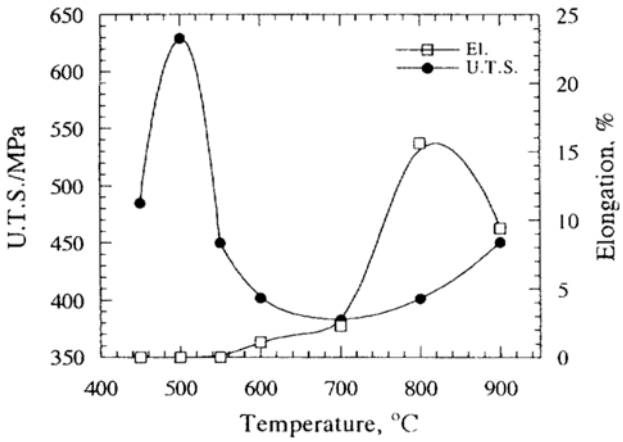

Fig. 3. Changes in ultimate tensile strength and elongation of the pure iron with aging temperature.

creased tensile strength, 485 MPa.

Fracture surfaces of the pure iron are shown in Figure 4. After aging at 700°C showing a minimum in ultimate tensile strength, the pure iron showed a typical intergranular fracture in which fracture paths followed prior austenite grain boundaries. Also, oxide particles could be found at the grain boundaries. The intergranular fracture mode considerably decreased after aging at 500°C, and hence the pure iron showed a mixed mode of intergranular and cleavage. According to the above results of the pure iron, the fracture mode of the pure iron in the range 500-700°C changed from intergranular to cleavage with increasing ultimate tensile strength. This means that the grain boundary cohesion increases with decreasing temperature.

Figure 5 shows grain boundary segregation behaviors in the pure iron of impurities with aging temperature. With decreasing temperature, carbon and nitrogen contents at the grain boundaries overally increased, but the sulfur content showed a decreasing tendency below 700°C. It is suggested that the change in sulfur content of the grain boundaries is attributed to the competitive segreagtion between sulfur and carbon or nitrogen. This suggestion can be partly supported by researches [62,63], which reported a competitive grain boundary segregation between the impurities in iron with varying bulk content.

Intergranular brittleness in the pure iron, when referred to Figures 3 and 5, is, as a result, due to the sulfur segregated at the grain boundaries. This has been confirmed also in several researches [60, 64, 65]. A role of carbon or nitrogen at the grain boundaries on the increased grain boundary strength may not be ignored in the present study. Briant [53] suggested that the decreasing tendency of sulfur below 700°C was due to

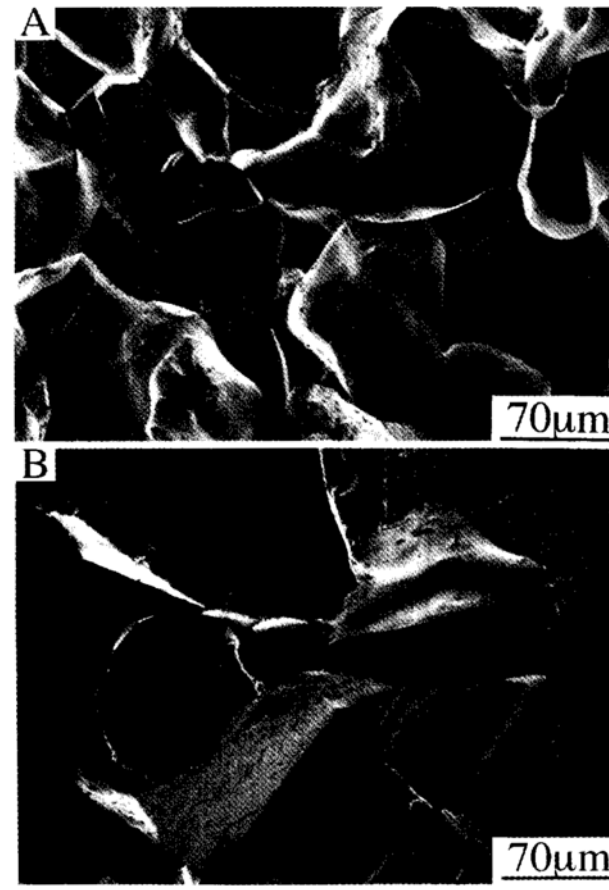

Fig. 4. Fracture surfaces of the pure iron: (a) aged at 700°C and (b) aged at 500°C.

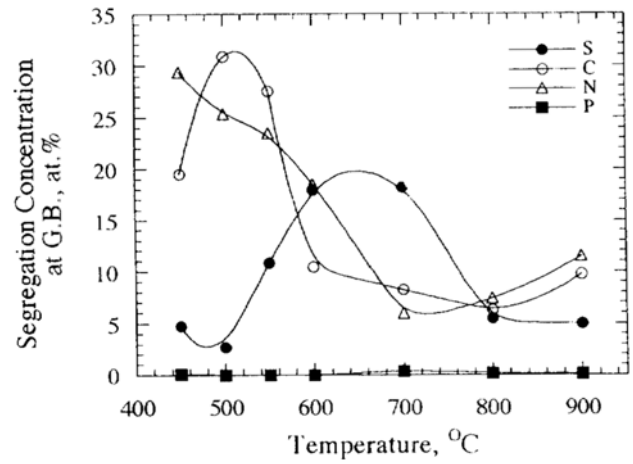

Fig. 5. AES analyses of the pure iron.

solubility limit of sulfur in pure iron and hence precipitation of iron sulfide followed by a loss in the matrix of sulfur. However, a recent study of pure iron [60] showed that the precipitate in pure iron is not sulfide but oxide. There are some evidences in the study that the de-

creasing tendency below 700°C of sulfur concentration at the grain boundaries with decreasing temperature is due to a competitive segregation between sulfur and carbon or nitrogen. Therefore, the Briant's suggestion [65] is not reasonable, when referred to the previous research [60].

Changes in hardness and ultimate tensile strength of the molybdenum-bearing alloy are shown in Figure 6. As in the pure iron, the molybdenum-bearing alloy also showed age-hardening behavior by oxide, which can be supported by Figure 2(b). Hardness levels were relatively high in comparison to those in the pure iron,

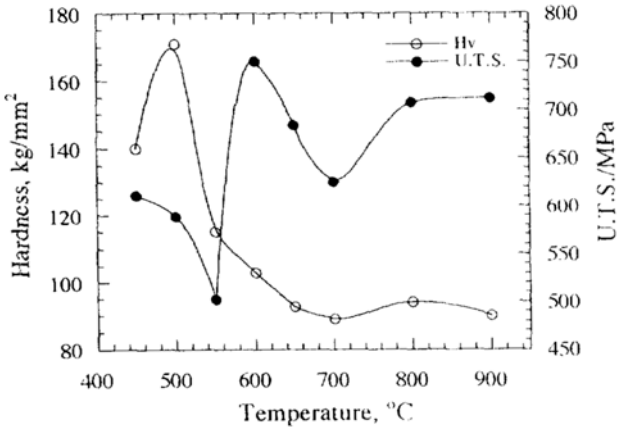

Fig. 6. Changes in hardness and ultimate tensile strength of the molybdenum-bearing alloy.

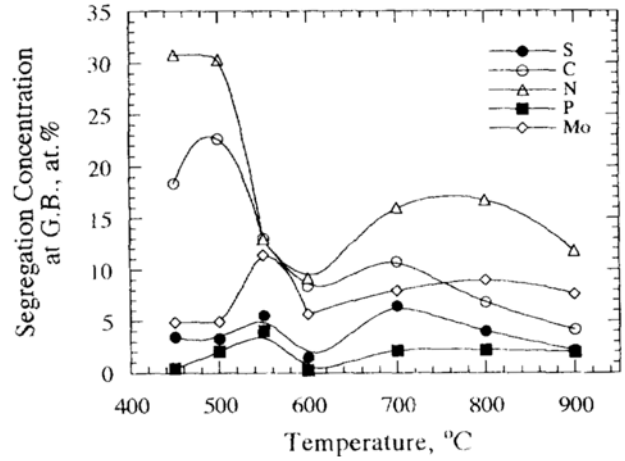

Fig. 8. AES analyses of the molybdenum-bearing alloy.

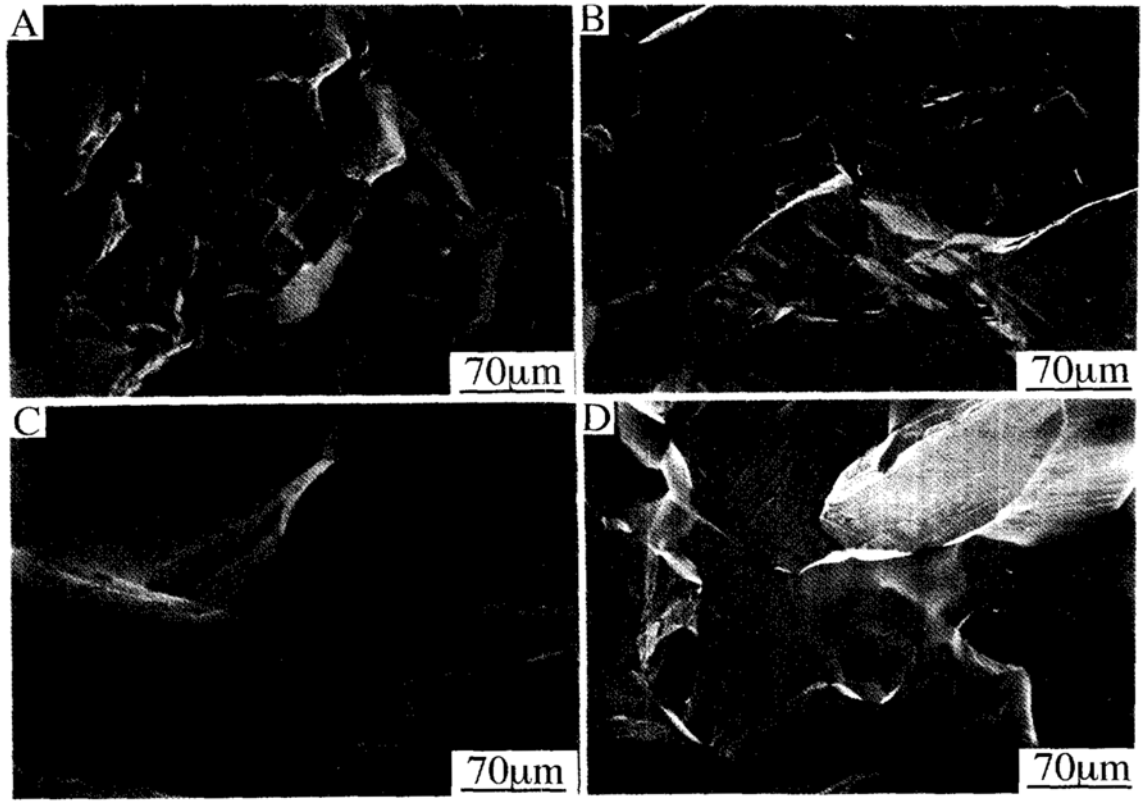

Fig. 7. Fracture surfaces of four alloys: (a) the molybdenum-bearing alloy aged at 600°C, (b) the 3.37 wt.%Si alloy aged at 600°C (for the rolling direction), (c) the 3.37 wt.%Si alloy aged at 600°C (for the transverse directrion) and (d) the aluminum-bearing alloy aged at 900°C.

and the temperature showing a maximum hardness level, 500°C, was not in accordance with that in the pure iron. As shown in Figure 7(a), the molybdenum-bearing alloy showed mostly transgranular fracture with nil ductility after aging at all the temperatures. As shown in Figure 6, changes in ultimate tensile strength with aging temperature are more complicated, relatively to those in the pure iron. Most of the tensile strength levels were much higher than those in the pure iron. Two troughs of tensile strength appeared at 550 and 700°C, and the tensile strength at 550°C, 502 MPa, was the lowest in this alloy. The maximum tensile strength with 750 MPa was obtained at 600°C. In the molybdenum-bearing alloy, the sulfur content at the grain boundaries prominently decreased in comparison to that in the pure iron, as shown in Figure 8, but the segregation behaviors of carbon and nitrogen were similar to those in the pure iron. The changes at the grain boundaries of sulfur content with aging temperature are generally consistent with those in tensile strength. That is, the grain boundary cohesion of the molybdenum-bearing alloy is directly influenced by the sulfur content at the grain boundaries. An intrinsic effect of molybdenum at the grain boundaries on the grain boundary cohesion can be found from a comparison between Figures 6 and 8. The phosphorus content at the grain boundaries of the molybdenum-bearing alloy seems to be higher than that of the pure iron, but this may be attributed to the overlap between the molybdenum 120 and phosphorus 120 eV peaks.

Figure 9 shows changes in hardness and ultimate tensile strength of the 3.37 wt.%Si alloy. The solid solution hardening effect of silicon was prominent in the alloy, as in other research [66], and, as a result, the hardness levels with the range 186 and 220 Hv were quite high, in comparison to that of the pure iron. The hardness decreased with decreasing temperature, and the decreasing extent was not big. The ultimate tensile strengths were within the range 130 and 334 MPa, and were overally lower than those in the pure iron. Nonetheless, the fracture mode of the silicon-bearing alloy, as shown in Figure 7(b), were mostly transgranular. This implies that, due to the relatively low cleavage fracture strength, the fracture in the silicon-bearing alloy is governed by cleavage strength rather than by intergranular fracture strength. Cleavage facets of the fracture surfaces were relatively flat and exhibited "river" lines that are generally associated with the cleavage process [67, 68]. In as-rolled condition, the silicon-bearing alloy, however, showed a typical intergranular fracture. As shown in Figure 7(c), the fracture mode in the transverse direction was mostly intergranular.

Surface analyses by AES were also performed on sam-

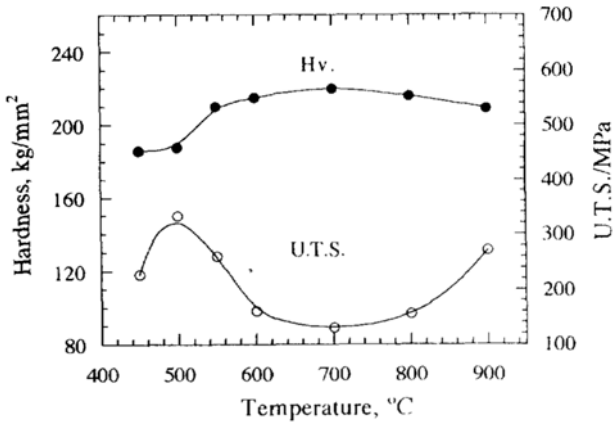

Fig. 9. Changes in hardness and ultimate tensile strength of the 3.37 wt.%Si alloy.

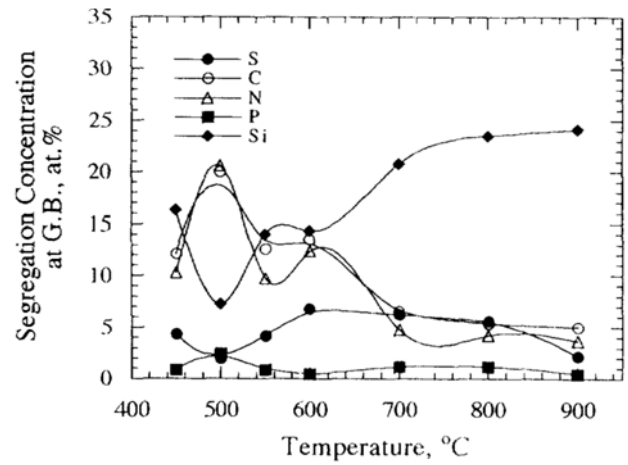

Fig. 10. AES analyses of intergranular fracture facets of the 3.37 wt.%Si alloy.

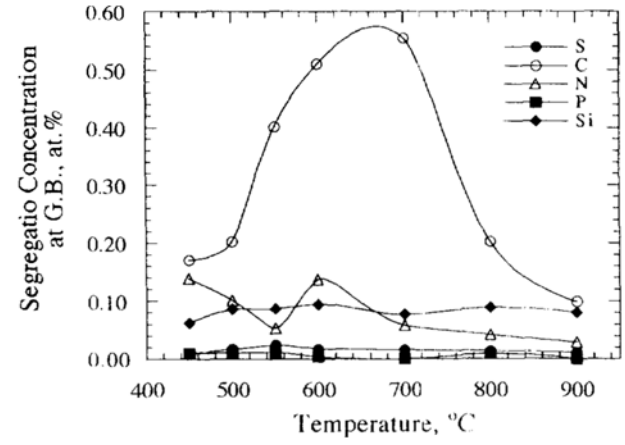

Fig. 11. AES analyses of the 4.26 wt.%Si alloy.

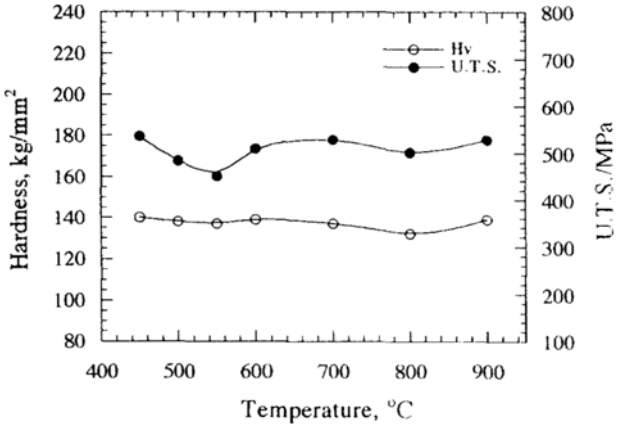

Fig. 12. Mechanical properties of the aluminum-bearing alloy.

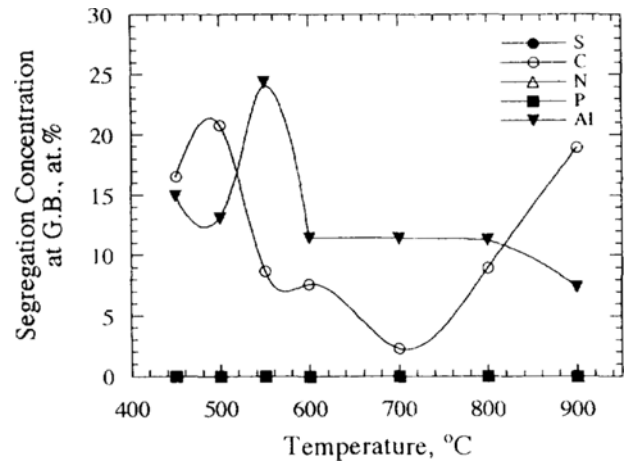

Fig. 13. AES analyses of the aluminum-bearing alloy.

ples machined from the tensile specimens of the 3.37 wt.%Si alloy, and the result is shown in Figure 10. The sulfur content was considerably decreased by the silicon addition. Competitive grain boundary segreagation behaviors between sulfur or silicon and carbon or nitrogen [21-29, 69] were also observed in the alloy.

In order to investigate the effect of increased silicon in the matrix on the grain boundary segregation behaviors of elements, an Fe-4.26 wt.%Si alloy with relatively high content of silicon was additionally prepared in the present study. Figure 11 shows changes in grain boundary segregation content of elements. The increased silicon content in the matrix caused the strong repulsion of sulfur and nitrogen at the grain boundaries, in comparison to that shown in Figure 10. After aging at 600 and 700°C, the carbon at the grain boundaries was extremely high. The silicon contents at the grain boundaries were not higher than those shown in Figure 10, and were insensitive to temperature.

Figure 12 shows the mechanical properties of aluminum-bearing alloy after aging at several temperatures. The solid solution hardening by aluminum was considerable, though the effect was not higher than that by silicon. The hardness did not nearly vary with aging temperature and was held at about Hv 140. The tensile strength also did not show a big difference with aging temperature and was in the range 451 and 536 MPa. The aluminum-bearing alloy showed intergranular fracture at all the temperatures, as shown in Figure 7(d). Sulfur and nitrogen at the grain boundaries were, as shown in Figure 13, completely removed by the addition of aluminum, and thus carbon and aluminum only were detected at the grain boundaries. The intergranular fracture strengths with no sulfur of the aluminum-bearing alloy were not high, in comparison to those with small amounts of sulfur of the pure iron, and were not largely influenced by the carbon content at the grain boundaries. This is due to the intrinsic embrittling effect of aluminum segregated at the grain boundaries, which was suggested in the Seah's pair bonding theory [70] and was indirectly showed in a research [71].

5. DISCUSSION

5.1. Main embrittling impurities: S, P, Sb and Sn

Before Auger electron spectroscopy was not available there was circumstantial evidence that sulfur caused grain boundary embrittlement in iron [72-74]. Auger experiments confirmed that sulfur is indeed a very common and potent embrittler in iron [73, 75] and that even at bulk concentrations of 10 wt. ppm significant amounts of sulfur could be found at the grain boundaries [76-78]. Phosphorus has been known to be an embrittler from the early study of temper embrittlement [79]. However, it is a considerably less potent embrittler than sulfur [80, 81]. The intrinsic effect of sulfur on the grain boundaries has been confirmed through the present study of various alloy systems.

Antimony and tin are much more powerful embrittling elements than phosphorus. However, they are only effective in steels that contain several percent of nickel, which is believed to enhance the intergranular segregation of these elements by virtue of an attractive interaction between the nickel and the impurities in an iron matrix. This effect has been rationalized by the Guttmann regular-solution model [33, 82]. In the absence of nickel, these elements do not cause temper embrittlement even at a level of several hundred wt. ppm

[83]. Such elements were not found at the grain boundaries of the present alloys with no nickel.

5.2. Carbon effect on grain boundary cohesion

Carbon strongly segregates to the grain boundaries of Fea [84], and interacts with many elements. In steels its behavior is extremely complicated since its concentration, much larger than that of impurities, is well in excess of the solubility limit, and both the soluble and precipitated carbon are involved in the segregation and mechanical properties. Carbon can also play a synergistic effect in the segregation process. Due to the very large M-C interaction, the already large intergranular concentration of carbon amplifies that of M, which in turn enhances those of impurities. It can be thought that the very deleterious effect induced by the association of nickel and chromium in temper-brittle steels may be due to an effect of this kind. However, the segregation of carbon decreases the intergranular brittleness of bcc iron by intrinsically increasing the cohesion of the grain boundary, and not by inhibiting the segregation of deleterious impurities [85, 86]. When the carbon solubility limit is exceeded, embrittlement increases again in iron [86] as in steels [87], but it is then associated with the purely mechanical role of the carbides in initiating fracture [73, 88, 89] or in increasing the hardness of the matrix [86].

Based on the present results, the carbon effect on the grain boundary cohesion can be different from that in the researches [85, 86]. The highest fracture strength level of the pure iron corresponded to the lowest sulfur and highest carbon contents at the grain boundaries. There is, therefore, a possibility that the carbon has intrinsically strengthened the grain boundaries. However, the intergranular fracture strengths in the aluminum-bearing alloy, where the sulfur has been completely repeled at the grain boundaires, have been lowered only by the aluminum segregated, and were not largely influenced by the wide changes in carbon content of the grain boundaries. As a result, the intrinsic carbon effect on intergranular cohesion is, if any, not big in the present alloy systems.

5.3. Embrittling effect of alloying elements: Mn, Ti, Al and Si

Studies for intrinsic effect of alloying elements on grain boundary cohesion have been little performed. Floreen and Speich [71] observed that Fe-Ni-Co quaternary maraging steels containing Mn, Ti, Al and Si showed intergranular brittleness and that high strength and high toughness were obtained in maraging steels containing Mo, Nb and Be. However, such mechanical behaviors in their alloys were not clearly understood.

It was reproted in the work of Steven and Balajiva [90] that manganese was an embrittling element in low manganese alloys, and their work was later supported by other researches [2, 86]. Squire and Wilson [91] suggested that the brittleness suffered in an Fe-6Mn-12Ni alloy was the result of segregation of manganese to the prior austenite grain boundaries. Alternatively, it was suggested that the effect of Mn was to increase the embrittling effects of impurities due to the interaction between manganese and impurities in low alloy steels with low levels of impurities [92].

Heo and Lee [42, 93] have quantitatively investigated the brittleness in Fe-Mn-Ni precipitation hardening alloys, and have concluded that the brittleness is due to the manganese segregated at the grain boundaries. Their conclusion is supported by the Heo's following research [43] based on a regular solution model, which has been theoretically performed in order to confirm the segregation behavior of manganese in the alloys. Heo has additionally reassessed the intergranular brittleness in an Fe-Ni-Ti precipitation hardening alloy [44]. His results show that the brittleness in the titanium-bearing alloy is caused by the titanium segregation and are not related to impurities.

Effect of grain boundary segregation of Si on intergranular cohesion was little investigated except a few papers [9, 94] of secondary hardening steels, which suggested a possible role of Si on intergranular fracture behaviors. In spite of most cleavage fracture in the rolling direction of the present 3.37- and 4.26 wt.%Si alloys, the intergranular fracture behaviors in the transverse direction and in the as-rolled condition probably implies a detrimental role of silicon on the intergranular cohesion.

On the other hand, fracture phenomena in Fe-Si alloys were interpreted in terms of the nucleation of microcracks by the initial formation of deformation twins. Hull [95] observed that a coarse-grained 3.25% Si alloy twinned and fractured simultaneously when tested in tension at 78 K. He considered that twinning nucleated cleavage and that the fracture stress was determined by the stress required to cause twinning. Hull [96, 97] and Honda [98] demonstrated that Fe-Si single crystals strained in tension in the [001] direction at 78 K twinned and fractured concomitantly. The disposition of twins in broken specimens suggested that the (001) cleavage cracks could have been initiated at the intersection of suitable

pairs of twins.

Roles of aluminum on grain boundary segregation and hence on intergranular cohesion can be shown in Figures 12 and 13. Some addition of aluminum to the pure iron resulted in no sulfur at the grain boundaries. However, the overall intergranular fracture strength (about 500 MPa) were rather lower than that corresponding to the minimum level of sulfur in the pure iron (630 MPa). This is due to an intrinsic role of aluminum, which may have had a detrimental effect on intergranular cohesion.

5.4. Strengthening elements: Mo, Nb and Be

The beneficial effect of molybdenum has been well known in multicomponent systems. However, whether this has to do with an enhancement of carbon segregation by the strong carbide-forming element [3], or whether it is an intrinsic strengthening effect by the element, has not been clearly understood, because of little study of the molybdenum role in simple systems. The intrinsic role of molybdenum can be shown in the present study of Fe-Mo alloy. When molybdenum is added to the pure iron, the sulfur content at the grain boundaries is overally lowered, as shown in Figure 8. However, the intergranular fracture strengths of the alloy (Figure 6) are higher in comparison to those at the grain boundaries with similar contents of sulfur of the pure iron (Figure 3).

Such a point of view of the intrinsic effect of molybdenum may be applied to the results of Fe-Ni-Co-X quaternary alloys [71]. Additionally, Seah's pair bonding theory [70], which suggests a general scheme of embrittling and remedial elements in a matrix, can be a reference for determining the intrinsic effect of elements in the matrix.

6. CONCLUSIONS

Grain boundary segregation and intergranular fracture in pure iron and ferrite containing molybdenum, silicon or aluminum have been investigated by using AES and tensile test. The results are summarized as follows:

(1) Competitive segregation between sulfur and carbon or nitrogen, which caused the decrease below 700°C of sulfur content at the grain boundaries, was observed in the pure iron. The intergranular brittleness was mainly caused by the sulfur segregated at the grain boundaries.

(2) When molybdenum was added to the pure iron, the sulfur contents at the grain boundaries were lowered in comparison to those in the pure iron, and the overall fracture strength was considerably increased, relatively. This arises from the intrinsic effect of molybdenum on the grain boundaries as well as the decrease in sulfur content of the grain boundaries.

(3) In the 3.37 wt.%Si alloy, silicon and carbon or nitrogen competitively segregated to the grain boundaries, and such a competitive segregation was observed also between sulfur and carbon or nitrogen. The sulfur content at the grain boundaries decreased with increasing silicon content. The fracture modes in the 3.37- and 4.26 wt.%Si alloys were transgranular in the rolling direction, but were mostly intergranular in the transverse direction and in the as-rolled condition. The intergranular characteristic in the fracture behavior may be attributed to the detrimental effect of silicon as well as sulfur on the intergranular cohesion.

(4) Carbon and aluminum only were found at the grain boundaries of the aluminum-bearing alloy. This suggests that aluminum is a strong repulser at the grain boundaries of sulfur. Also, it was found that aluminum has a detrimental effect on grain boundary strength of ferrite.

APPENDIX

The emitted Auger electrons are detected by an electron spectrometer with transmission efficiency, $T(E_b)$, and an electron detector of efficiency, $D(E_b)$. For pure bulk i, the intensity $I_{i,0}$ of Auger electrons is given by

$$I_{i,0}=k\int_0^{\infty}(1+r_{i,0})I_i^0\exp\left(\frac{-z}{\lambda_{i,e}}\right)dz$$
$$=k(1+r_{i,0})I_i^0\lambda_{i,e} \qquad \text{(A1)}$$

where k equals $T(E_b)D(E_b\sigma(E_p)$, $\sigma(E_p)$ is the cross section for excitation of electrons of the studied kind, E_p and E_b each are the primary beam energy and the binding energy (i.e. Auger peak energy), $r_{i,0}(E_p, E_b, \alpha)$ is the backscattering factor of the pure element which is zero for X-ray photoelectron spectroscopy (XPS), α is the angle to the surface normal of the incident electron beam, I_i^0 is the primary electron intensity and $\lambda_{i,e}$ is the effective escape depth of i (in monolayers) expressed by

$$\lambda_{i,e}=\lambda_i\cos\theta \qquad \text{(A2)}$$

where λ_i is the inelastic mean free path (IMFP) of i Auger electrons, υ is the emission angle of detected electrons with respect to the surface normal of sample.

Let us consider a bulk which is homogeneous, except the top surface (i.e. a monolayer randomly mixed with

different kinds of N elements). That is, the monolayer segregation approach is chosen to derive an expression for the determination of the surface composition. Mole fractions in the monolayer and in the homogeneous bulk consisting of N elements each are f_X, f_Y, f_Z, $\cdots$, f_N and $f_{X,0}$, $f_{Y,0}$, $f_{Z,0}$, $\cdots$, $f_{N,0}$. The Auger electron intensity of an element X is expressed by

$$I_X = k\int_0^1 (1+r_{X,N}) f_X I_X^0 \exp\left(\frac{-z}{\lambda_{X,e}}\right) dz + k\int_1^\infty (1+r'_{X,N}) f_{X,0} I_X^0 \exp\left(\frac{-z}{\lambda_{X,e}}\right) dz. \quad \text{(A3)}$$

Similarly, the Auger electron intensity of the matrix is given by the following equation:

$$I_M = k\int_0^1 (1+r_{M,N})\left(1-\sum_{X\neq M}^{N} f_X\right) I_M^0 \exp\left(\frac{-z}{\lambda_{M,e}}\right) dz = k\int_0^\infty (1+r'_{M,N})\left(1-\sum_{X\neq M}^{N} f_{X,0}\right) I_M^0 \exp\left(\frac{-z}{\lambda_{M,e}}\right) dz. \quad \text{(A4)}$$

Evaluations of the backscattering factor [46, 99-102] have been made by several authors by Monte Carlo calculations, and empirically by Reuter [103]. THe calculations are roughly in agreement for deep cores levels but Ruther's relation errs on the low side for core levels below 500eV. Shimizu and Ichimura's [46, 102] calculations are most complete:

$$r_{i,N} = (2.34 - 2.10Z^{0.14})U^{-0.35} = (2.58Z^{0.14} - 2.98) \quad \text{(for } \alpha = 0°\text{)} \quad (5)$$

where U is the over-voltage ratio of the primary energy to the binding energy ($U=E_p/E_b$), Z is the mole fraction weighted mean atomic number of a layer which is given by

$$Z = \sum_j X_j Z_j. \quad \text{(A6)}$$

In the well-established electron probe microanalysis (EPMA) literature the backscattering factor for a compound or mixture is simply derived by the sum of the product of the weight fraction of each element times its backscattering factor [104]. However, Ichimura and Shimizu merely use the mole fraction weighted mean Z value to determine the backscattering factor. The functional dependence of r and Z in practice makes both procedures similar and, at present, the experimental data have not the precision to determine which is correct.

The concentration dependence of the backscattering factor was usually neglected [1, 105, 106]. In a multicomponent system, the Z and the backscattering factor r are expressed with the multicomponents, and this makes the quantification process difficult. Therefore, the backscattering factors in equations (A1), (A3) and (A4) are, for simplicity, approximated in quantitative AES as follows:

$$r_{X,0} \cong r_{X,N} \cong r'_{X,N} \quad \text{(A7)}$$

Then, equations (A3) and (A4) reduce to equation (15) in the text.

REFERENCES

1. E. D. Hondros and M. P. Seah, *Int. Met. Rev.* **22**, 262 (1977).
2. B. J. Schultz and C. J. McMahon, Jr., in *Temper Embrittlement of Alloy Steels*, p. 104, ASTM STP **499** (1972).
3. M. Menyhard and C. J. McMahon, Jr., *Acta Metall.* **37**, 2287 (1989).
4. Ph. Dumoulin, M. Guttmann , M. Palmier, M. Wayman, M. Biscondi, *Met. Sci.* **14**, 1 (1980).
5. C. J. McMahon, Jr., A. K. Cianelli and J. C. Feng, *Metall. Trans.* **8A**, 1055 (1977).
6. J. Yu and C. J. McMahon, Jr., *Metall.Trans.* **11A**, 291 (1980).
7. C. J. McMahon, Jr., Y. Q. Weng, M. J. Morgan and M. Menyhard, *Grain Boundary Structure and Related Phenomena* (1986).
8. R. O. Ritchie, Metall. *Trans.* **9A**, 35 (1978).
9. M. S. Bhat, W. M. Garrison and V. F. Zackay, *Mater. Sci. Eng.* **41**, 1 (1979).
10. Y. X. Zhou, S. C. Fu and C. J. McMahon, Jr., *Metall. Trans.* **12A**, 959 (1981).
11. Y. X. Zhou, C. J. McMahon, Jr. and E. W. Plummer, *J. Vac. Sci. Technol.* **2**, 1118 (1984).
12. F. Bezuidenhout, J. du Plessis and P. E. Viljoen, *J. Vac. Sci. Technol.* **2**, 1481 (1984).
13. H. de Rugy and H. Viefhaus, *Surf. Sci.* **173**, 418 (1986).
14. M. Es-Souni and A. Mosser, *Scripta Metall.* **22**, 1469 (1988).
15. P. Lejcek, V. Paidar and M. Koutnik, *Scripta Metall.* **22**, 1379 (1988).
16. M. Es-Souni and A. Mosser, *Surf. Sci.* **199**, 439 (1988).
17. P. Lejcek, M. Koutnik, J. Bradler, V. Paidar and A. Potmesilova, *Appl. Surf. Sci.* **44**, 75 (1990).
18. P. Lejcek and S. Hofmann, *Acta Metall.* **39**, 2469 (1991).
19. W. C. Leslie and G. C. Rauch, *Metall. Trans.* **9A**, 343 (1978).

20. J. W. Gibbs, *The Scientific Papers of J. Willard Gibbs*, Vol. 1, p. 219, Dover, New York (1961).
21. D. McLean, *Grain Boundaries in Metals*, Chap. V, Oxford Univ. Press, London (1957).
22. R. Defay, I. Prigogine, A. Bellemans and D. H. Everett, *Surface Tension and Adsorption*, p. 158, Wiley, New York (1966).
23. J. L. Meijering, *Acta Metall.* **14**, 251 (1966).
24. R. A. VanSanten and W. M. H. Sachtler, *J. Catalysis* **33**, 202 (1974).
25. F. L. Williams and D. Nason, *Surface Sci.* **45**, 377 (1974).
26. K. Binder, D. Stauffer and V. Wildpaner, *Acta Metall.* **23**, 1191 (1975).
27. V. S. Sundaram and P. Wynblatt, *Surface Sci.* **52**, 569 (1975).
28. J. J. Burton, E. Hyman and D. Fedak, *J. Catalysis* **37**, 106 (1975).
29. P. Wynblatt and R. C. Ku, *Surface Sci.* **65**, 511 (1977).
30. J. Friedel, *Advan. Phys.* **3**, 446 (1954).
31. M. P. Seah and E. D. Hondros, *Proc. R. Soc. Lond.* **A 335**, 191 (1973).
32. R. P. Gupta and B. Perraillon, *Surf. Sci.* **103**, 397 (1981).
33. M. Guttmann, *Surf. Sci.* **53**, 213 (1975).
34. M. P. Seah, *Acta Metall.* **25**, 345 (1977).
35. M. Guttmann and D. McLean, in *Interfacial Segregation* (eds., W. C. Johnson and J. M. Blakely), p. 261, Am. Soc. Metals, Metals Park, Ohio (1979).
36. J. Yu and C. J. McMahon, Jr, *Metall. Trans.* **11A**, 277 (1980).
37. C. Lea and M. P. Seah, *Phil. Mag.* **35**, 213 (1977).
38. S. Hofmann and J. Erlewein, *Surf. Sci.* **77**, 591 (1978).
39. G. Rowland s and D. P. Woodruff, *Phil. Mag.* **40**, 459 (1979).
40. C. Lea and M. P. Seah, *Met. Sci.* **18**, 521 (1984).
41. K. Abiko, S. Suzuki and H. Kimura, *Trans. Japan Inst. Metals* **23**, 43 (1982).
42. N. H. Heo, *Metall. Trans.*, (in press).
43. N. H. Heo, *Acta Metall.*, **44**, 1581 (1996).
44. N. H. Heo, *Acta Metall.*, (in press).
45. L. E. Davis, N. C. MacDonald, P. W. Palmberg, E. Riach and R. E. Weber, *Handbook of Auger Electron Spectroscopy, 2nd edn. Physical Electronics*, Edina, Minnesota (1976).
46. R. Shimizu, *Japanese J. Applied Physics* **22**, 1631 (1983).
47. E. D. Hondros and M. P. Seah, *Int. Met. Rev.* **222**, 262 (1977).
48. M. P. Seah, in *Practical Surface Analysis by Auger and X-ray Photoelectron Spectroscopy* (eds., D. Briggs and M. P. Seah), p. 181, Wiley, New York (1983).
49. L. Marchut and C. J. McMahon, Jr., in *Electron and Positron Spectroscopies in Materials Science and Engineering* (eds., O. Buck, J. K. Tien and H. L. Marcus), p. 183, Academic Press, New York (1979).
50. P. Dumoulin and M. Guttman, *Mater. Sci. Eng.* **42**, 249 (1980).
51. J. C. Bertolini, J. Massardier, P. Delichere, B. Tardy and B. Melik, *Surf. Sci.* **119**, 95 (1982).
52. F. Pons, J. Lehericy and J. P. Langeron, *Surf. Sci.* **69**, 565 (1977); G. Lorang, M. DaCunha Belo and J. P. Langeron, *J. Vacuum Sci. Technol.* **5A**, 1213 (1987).
53. J. Cazaux, P. Etienne and M. Razeghi, *J. Appl. Phys.* **59**, 3598 (1986).
54. H. Iwasakin and S. Nakamura, *Surf. Sci.* **57**, 779 (1976).
55. M. P. Seah, *Surf. Sci.* **32**, 703 (1972).
56. J. C. Shelton, *J. Electron Spectrosc.* **3**, 417 (1974).
57. M. P. Seah and W. A. Dench, *Surf. and Interf. Anal.*, **1**, 2 (1979).
58. G. W. C. Kaye and T. H. Laby, *Tables of Physical and Chemical Constants*, 14th edn. Longman, London (1973).
59. R. C. Weast (ed.), *Handbook of Chemistry and Physics*, 58th edn. CRC Press, cleveland, Ohio (1977-78).
60. N. H. Heo, *Acta Metall.*, (revised).
61. R. Honda and H. Taga, *Metal Sci.* **2**, 172 (1968).
62. G. Tauber and H. J. Grabke, Ber. Bunsenges. *Phys. Chem.* **82**, 298 (1978).
63. S. Suzuki, S. Tanii, K. Abiko and H. Kimura, *Metall. Trans.* **18A**, 1109 (1987).
64. K. S. Shin and M. Meshii, *Acta Metall.* **31**, 1559 (1983).
65. C. L. Briant, *Acta Metall.* **33**, 1241 (1985).
66. W. B. Morrison adn W. C. Leslie, *Metall. Trans.* **4A**, 379 (1973).
67. J. R. Low, Jr., *Fracture*, p. 68. Wiley (1959).
68. J. R. Low, Jr., *Prog. Mater. Sci.* **12**, 1 (1963).
69. H. J. Grabke, *Steel Research* **57**, 178 (1986).
70. M. P. Seah, *Acta Metall.* **28**, 955 (1980).
71. S. Floreen and G. R. Speich, *Trans. ASM.* **57**, 714 (1964).
72. C. J. McMahon, Jr., *Acta Metall.* **14**, 839 (1966).
73. C. J. McMahon, Jr., in *Grain Boundaries in Engineering Materials* (eds., J. L. Walter *et al.*), p. 525, Claitor's Publ., Baton Rouge, Louisiana.
74. C. Pichard, J. Rieu and C. *Goux, Metall. Trans.* **7A**, 1811 (1976).
75. P. Jolly, *Metall. Trans.* **2A**, 341 (1971).
76. M. P. Seah and E. D. Hondros, *Proc. R. Soc. London Ser.* **A 335**, 191 (1973).
77. D. B. Powell, H. J. Westwood, D. M. R. Taplin and H. Mykura, *Metall. Trans.* **4A**, 2357 (1973).
78. G. Tauber and H. J. Grabke, *Ber. Bunsenges. Phys. Chem.* **82**, 298 (1978).

79. R. H. Greaves and J. A. Jones, *J. Iron Steel Inst.* **111**, 231 (1925).
80. P. V. Ramasubramanian and D. F. Stein, *Metall. Trans.* **4A**, 1735 (1973).
81. H. Erhart and H. J. Grabke, *Met. Sci.* **15**, 401 (1981).
82. R. A. Mulford, C. J. McMahon, JR., D. P. Pope and H. C. Feng, *Metall. Trans.* **7A**, 1296 (1976).
83. J. C. Murza and C. J. McMahon, Jr., *ASME J. Eng. Mater. Tech.* **102**, 369 (1980).
84. E. D. Hondros, *Met. Sci.* **1**, 36 (1967).
85. C. Pichard, J. Rieu and C. Goux, *Met. Trans.* **7A**, 1811 (1976).
86. Y. Q. Weng and C. J. McMahon, Jr., *Mater. Sci. Tech.* **3**, 207 (1986).
87. R. A. Mulford, C. J. McMahon, D. P. Pope and H. C. Feng, *Met. Trans.* **7A**, 1183 (1976).
88. C. J. McMahon and M. Cohen, *Acta Met.* **13**, 591 (1965).
89. E. Smith, *Physical Basis of Yield and Fracture*, p. 36, Institute of Physics and the Physical Society, H. M. S. O., London (1966).
90. W. Steven and J. Balajiva, *J. Iron and Steel Inst.* **193**, 141 (1959).
91. D. R. Squire and E. A. Wilson, *Met. Trans.* **3A**, 575 (1972).
92. J. D. Bolton, *Ph. D. Thesis*, Sheffield Polytechnic, (1970).
93. N. H. Heo, *Ph. D. Thesis*, Seoul National University, (1993).
94. R. O. Ritchie, *Metall. Trans.* **8A**, 1131 (1977).
95. D. Hull, *Acta Metall.* **9**, 191 (1961).
96. D. Hull, *Phil. Mag.* **3**, 1468 (1958).
97. D. Hull, *Acta Metall.* **8**, 11 (1960).
98. R. Honda, *J. Phys. Soc. Japan* **16**, 1309 (1961).
99. A. Jablonski, S. H. Overbury and G. A. Somorjai, *Surf. Sci.* **65**, 578 (1977).
100. M. M. El Gomati and M. Prutton, *Surf. Sci.* **72**, 485 (1978).
101. A. Jablonski, *Surf. Interface Anal.* **2**, 39 (1980).
102. S. Ichimura and R. Shimizu, *Surf. Sci.* **112**, 386 (1981).
103. W. Requer, in *Proceedings of 6th International Conference on X-ray Optics and Microanalysis* (eds., G. Shinoda, K. Kohra and T. Ichinokawa), p. 121, University of Tokyo Press (1972).
104. V. N. E. Robinson, N. G. Cutmore and R. G. Burdon, *SEM*, **II**, 483 (1984).
105. T. E. Gallon, *Surface Sci.* **17**, 486 (1969).
106. M. P. Seah, *Surface Sci.* **32**, 703 (1972).